Title: A comparative study on the physicochemical characteristics of nanoparticles released *in vivo* from CoCrMo tapers and cement-stem interfaces of total hip replacements

Authors: Alina M. Crainic[1], Mauro Callisti[2, 1], Arjen van Veelen[3,4], Agnes Michalik[5], James A. Milton[5], Martin R. Palmer[5], Richard .B. Cook[1]

Affiliation:

[1]National Centre for Advanced Tribology at Southampton (nCATS), University of Southampton, University Road, Southampton SO17 1BJ, United Kingdom;

[2]Department of Materials Science and Metallurgy, Cambridge University, 27 Charles Babbage Road, Cambridge, CB3 0FS, United Kingdom;

[3]Material Science and Technology Division, Material Science and Technology Division, Los Alamos, NM 87545,

[4]Stanford Synchrotron Radiation Lightsource, SLAC National Accelerator Laboratory, Menlo Park, CA 94025

[5]School of Ocean and Earth Science, National Oceanography Centre Southampton (NOCS), University of Southampton, European Way, Southampton SO14 3ZH, United Kingdom;

Corresponding author: Richard B Cook (R.B.Cook@soton.ac.uk)

Keywords: Orthopaedics, nanoparticles, TEM, Cobalt Chromium, Hip replacements

Abstract

The good biocompatibility and corrosion resistance of the bulk CoCrMo alloy has resulted in it being used in the manufacture of implants and load bearing medical devices. These devices, however, can release wear and corrosion products which differ from the composition of the bulk CoCrMo alloy. The physicochemical characteristics of the particles and the associated *in-vivo* reactivity are dictated by the wear mechanisms and electrochemical conditions at the sites of material loss. Debris released from CoCrMo hip bearings, taper junctions or cement-stem interfaces can therefore have different chemical and morphological characteristics which provides them with different *in-vivo* toxicities. Here, we propose to assess and compare the characteristics of the particles released *in-vivo* from CoCrMo tapers and cement-stem interfaces which have received less attention compared to debris originating from the hip bearings. The study uses state-of-art characterisation techniques to provide a detailed understanding of the size, morphology, composition and chemistry of the particles liberated from the wear and corrosion flakes from revised hip replacements, with an enzymatic treatment. The phase analyses identified Cr_2O_3 nanoparticles released from tapers and cement-stem interfaces, whose composition did not vary with origin or particle morphology. The size distributions showed significantly smaller particles were released from the stems, compared to the particles originating from the corresponding tapers. The investigation demonstrates that the tribocorrosive processes occurring at the taper and stem interfaces both result in Cr_2O_3 nanoparticle formation.

Introduction

The release of metal debris and corrosion products from total hip replacements can occur from taper junctions and cement stem interfaces, in addition to or independently of the wear from the bearing surfaces. The amount of debris released from the metallic secondary interfaces (i.e. tapers and cement-stem interface) is normally less than the amount of debris originating from the metal-on-metal (MoM) hip bearings[1]. The incidence of implant failure due to taper damage, however, is concerning and affects implants regardless of the bearing material combinations[2-10]. It is of particular concern when the femoral head and stem components used in combination are from 2 different manufacturers due to angle and tolerance mismatches[8, 11]. Moreover, the adverse local tissue reactions (ALTRs) to debris released from tapers are believed to be more aggressive than those initiated by similar doses of particles released from MoM bearing surfaces[12, 13]. A potential reason for that could be the different periprosthetic environments created by debris from the tapers and bearings, which may yield to different immunogenicity and adverse body reactions[13]. Despite the reports of wear and corrosion at the cement-stem interface[14-20], there is little evidence of ALTRs to debris originating from this particular wear site, and not much is known about how the particles compare to those released from tapers or CoCrMo bearing surfaces.

The release of material from the primary and secondary interfaces in total hip replacements is governed by different wear mechanisms and electrochemical conditions which may shape the particles and influence their physicochemical characteristics. CoCrMo taper junctions are subject to wear by mechanically assisted crevice corrosion (MACC) which results in both wear and corrosion products[21]. The release of debris from the cement-stem interface is usually initiated by micromotion which leads to tribocorrosion, and the formation of black deposits at the loose cement-stem interface [16, 17, 22, 23]. The process of wear and material release from the MoM bearing surfaces has been well documented and the characteristics of the associated debris have been previously studied [24-28]. The CoCrMo hip articulations are subject to abrasive wear and produce less volumetric debris compared to certain alternative bearings. The number of particles, however, is approximately 100 times higher than that produced from the polyethylene bearings, and the majority are in the nanometre size range[25, 26, 29, 30]. The small particle size of the metal debris means increased mobility and ability to travel systemically[31]. In fact, previous studies have shown evidence of debris originating from hip replacements and localised at distant organs, such as lymphatic nodes, liver, spleen, heart and brain[32-36]. Investigation of the biopsies from periprosthetic tissue or from distant organs

revealed mainly Cr oxides [27], Cr phosphates [27, 28, 32, 37] and CoCrMo debris [26, 32]. Others reported and characterised debris originating from MoM hip bearings, embedded in or liberated from periprosthetic tissue [26, 29, 37, 38], synovial aspirates or serum lubricants used in hip simulator studies [24, 25, 30, 39, 40]. The majority identified nano-sized Cr rich debris, either as oxides or phosphates, and CoCrMo particles.

Previous retrieval studies reported black wear and corrosion flakes around the CoCrMo tapers [3, 6, 32] and cement-stem interfaces [15, 17], which were shown by energy dispersive X-ray analysis (EDX) to contain mainly Cr and P, with traces of Co, Mo and other elements of biological origin [15-17, 32]. These flakes are micron-sized organo-metallic composites, comprising metal particles, corrosion products, precipitates and organic material [16]. Their investigation did not provide information about the actual size and composition of the nano-sized species which make up the large and flaky debris. A comprehensive characterisation, therefore, requires the digestion of the flakes to liberate the metal particles to understand about the modes of material loss and corrosion processes at the sites of wear. The investigation of debris released from CoCrMo tapers and cement-stem interfaces, internalised in periprosthetic tissue and macrophages, showed clusters of Cr oxides [14, 41-43], Cr phosphates [32, 43] and CoCr nanoparticles [14]. The harsh conditions in the lysosomal compartments (i.e. acidic pH ~4), however, may change the chemistry of the debris and thus misidentify the species released from the wear sites. Also, none of the previous studies attempted to liberate the aggregates from the host environment and digest them to release and characterise the individual metal particles. The lack of knowledge regarding the size, morphology, composition and chemistry of debris released from distinct wear sites, makes it difficult to assess the particle toxicity in relation to origin and understand why some particles are more reactive than others .

Here, we investigate debris released from two retrieved implants, each with signs of wear and corrosion at both the taper and cement-stem interface. The as-retrieved debris, collected and processed identically, allow therefore the direct and unbiased comparison of the metal particles released from the CoCrMo taper and cement stem interface of the same retrieval. By comparing sites on the same joints, the study eliminates the interpatient variabilities, such as local pH, host responses and immunological particularities that could have affected the biochemical conditions at the joint cavity and could have influenced the physicochemical characteristics of the particles originating from these wear sites. The main objective here was to compare the size distribution, composition and chemistry of the metal particles released *in vivo* from CoCrMo tapers and cement-stem interface and identify physicochemical differences that may result in

different *in vivo* reactivity and ALTRs. The detailed morphological, structural and chemical characterisation of the cleaned nanoparticles, liberated from the surrounding biological matrix with an enzymatic treatment, was performed using state-of-art electron microscopy techniques, such as high resolution scanning transmission electron microscopy (STEM) fitted with EDX and electron energy loss spectroscopy (EELS), transmission electron microscopy (TEM) and selected area electron diffraction (SAED), and scanning transmission X-ray microscopy (STXM) operated in X-ray absorption spectroscopy (XAS) mode.

Materials and methods

Patients and implants

The hip replacements were retrieved at Southampton General Hospital, with permission from donors and approval from the National Research Ethics Service Committee, South Central-Southampton A. The surgery followed the onset of patient reported pain and the diagnosis of ALTRs with abnormally high Co and Cr blood levels. The retrievals were large CoCrMo heads joined with cemented CoCrMo stems (mixed manufacturers), which both exhibited bearing wear scars and wear rates which were indicative of correct alignment in-vivo (details in Table 1). After retrieval, the explanted components were sterilised and stored in 10% buffered formalin, until further investigation.

RedLux Imaging

The loss of material from the female side of the taper (bore of the head) was investigated with a RedLux Artificial Hip Joint Profiler (RedLux, Southampton, UK). The instrument was described elsewhere and has the ability to perform ultra-precision three-dimensional (3D) form metrology, with a spatial resolution of 20 nm. The RedLux imaging of the female tapers was performed based on replica casting made using Microset 101RF (Microset Products, Ltd, Nuneaton, UK), capable to reproduce fine details to a resolution down to 0.1 µm.

Debris recovery

The retrievals presented signs of wear and corrosion at the base of the trunnion and in the proximal region of the cemented stems (Figure 1). To avoid the accidental damage of the metal surfaces, the loose wear and corrosion flakes were removed from around the revised tapers and cement-stem interfaces with plastic tweezers and collected in clean plastic tubes. Because the

retrievals had been exposed to atmospheric humidity and oxygen prior to the collection, no special storage conditions were granted to the recovered flakes either.

ICP-MS analysis

After retrieval, a fragment of each corrosion flake was weighed in Teflon digestion vessels and subject to a sequential overnight digestion in Aqua Regia at 130°C, followed by HNO_3/H_2O_2 at 130°C. The dissolved samples were evaporated to dryness and redissolved in 3% HNO_3 and spiked with 1 ppb of In and Rh, as internal standards. Mass spectrometry was performed using an HR-ICP-MS Thermo Fisher Scientific Element XR (Bremen, Germany). Data were acquired using medium resolution via PFA nebuliser and cyclonic spray chamber. After each sample analysis, a wash solution containing 3% HNO_3 was run until background levels were achieved. The raw data were blank and internally corrected and then calibrated against synthetic standards (Inorganic Ventures, Virginia, USA).

Enzymatic digestion

The digestion of the flakes and the release of clean metal nanoparticles was performed using an enzymatic protocol[44]. The method involved a 24 hrs incubation of the solid flakes (~0.8 mg) with 0.25 mg lyophilised Papain (Sigma Aldrich, UK) in 2 ml 50 mM Tris-HCl, at 65°C, under continuous stirring at 180 rpm. The pellets (metal debris) were then recovered by centrifugation at 50,000 x g and were subject to a second incubation with 0.8 mg Proteinase K (Sigma Aldrich. UK) in 2 ml 50 mM Tris-HCl, for 24 hrs, at 55°C. Before each incubation, the debris was washed with 2 ml 2.5% sodium dodecyl-sulphate (SDS) (Sigma Aldrich, UK) and subject to ultrasound for 15 mins. The particles were finally recovered by centrifugation at 50,000 x g (Optima MAX-XP, Beckman Coulter, TLA-55 fixed angle rotor), washed twice with 2 ml deionised water (DIW) and stored in 100-200 μl DIW at -20°C, prior to further analysis.

Electron Microscopy

Particles displayed on carbon-coated copper grids were characterised with a high-resolution Cs probe-corrected JEOL ARM200F (cold-FEG) TEM/STEM operated at 200 kV and equipped with a 100 mm^2 Centurion EDX detector (Thermo Fisher Scientific Inc., Madison, Wisconsin, USA) and electron energy loss spectrometer (EELS)[44]. EELS data were acquired in STEM mode by using an energy dispersion of 0.1 eV/channel and a collection and convergence semi-angles of 40 and 30 mrad respectively. Prior quantitative elemental analyses, EELS data were

corrected for energy drift by using the low-loss energy spectrum acquired on the same region of the corresponding core-loss energy spectrum. SAED patterns of the samples and Cr_2O_3 standard (Fisher Scientific) were acquired with a JEOL JEM-2100 operated at 200 kV. Gatan Digital Micrograph was used to process the acquired STEM micrographs, EELS data and SAED patterns while NSS 4 X-Ray Microanalysis software (Thermo Scientific) was used to process the EDX data.

Scanning Transmission X-ray Microscopy (STXM) and XANES

The speciation analysis was performed using the STXM at beamline I08 at Diamond Light Source Ltd. (Harwell, Science and Innovation campus, UK). This beamline uses soft X-ray radiation in the 250-4200 eV photon energy range and can achieve a lateral resolution of ~20 nm, depending on the imaging mode. The XANES spectra were recorded over five energy regions, from 572 to 598 eV, covering the characteristic Cr $L_{2,3}$-edges, at an energy step of 1 eV for the first and last energy ranges, and a step of 0.2 eV for the middle (576-593 eV) intervals. The characteristic XANES spectrum of the standard Cr_2O_3 and CrH_8O_8P samples (Fischer Scientific) were used for the linear combination fitting of the recorded spectra of the particle clusters, using Athena 0.9.25.

PSD and Statistical Analysis

PSD and morphological characterisation was performed according to BS ISO 17853/2011. The STEM micrographs were processed with Gatan Digital Micrograph software, to measure the maximum dimension (d_{max} or length, the longest straight line between two opposite points on the particle outline) and maximum orthogonal dimension (d_{min} or width) of the particles. The maximum diameter (d_{max}) was used to define the PSD, while the d_{max}/d_{min} value, hereafter referred to as the aspect ratio (AR), was used for morphological characterisation. The particles were considered round for $1 \leq AR < 1.5$, oval for $1.5 \leq AR < 2.5$ and needle shaped for $AR \geq 2.5$. The statistical significance of the data sets was verified using the null hypotheses statistical tests (F-test and two-sample T-test), at a level of confidence of 0.05.

Results

RedLux Imaging

Figure 2 represents the height maps for cases 1 and 2, showing the deviation of tapers from their initial geometry, as a result of wear and corrosion. The original surface is preserved for

2-3 mm at the proximal and distal end of the tapers, appearing in green for Case 1, and yellow for Case 2, while the regions affected by material loss are in blue, purple or black.

The mechanism of damage differs between the cases. In Case 1, the damage is uniformly distributed around the circumference and along the length of the taper-trunnion overlap, with a ring of material loss around the distal open end of the taper-trunnion overlap, likely due to a corrosion-dominated process. The total volumetric loss from the female taper in Case 1 was 3.291 mm^3, with a maximum depth of the wear scar of 25.75 µm.

The taper damage profile in Case 2 demonstrates that a toggling motion occurred between the taper and the trunnion, characterised by the deepest points of loss being at the distal end of the 0^o and the proximal end of the 180^o images in Figure 2. The most affected region was the distal region of the taper-trunnion contact with a maximum depth of 19.9 µm and a total volumetric material loss of 3.479 mm^3.

ICP-MS

The compositions of the as-retrieved flakes, determined using ICP-MS analysis, are shown in Table 2. Debris collected from the cement-stem interfaces and from around taper 2 contained mainly Cr, but also Co and Mo. The flake retrieved from around taper 1 contained more Co and Mo than Cr. The total amount of metal (Cr, Co and Mo) varied between the samples and ranged from 13.9%, for debris from stem 2, to 37.9%, for debris from taper 2. The difference to 100% is represented by non-metallic species or precipitates, originating from the body. No trend was observed for the proportions of the main elements in relation to the origin of debris (tapers or cement-stem interface).

Electron Microscopy

The morphology of the digested debris, released *in vivo* from the CoCrMo taper junctions and cement-stem interfaces is shown in Figure 3. The enzymatic treatment resulted in both partially digested flakes (Figure 3A-D) and individual nano-particles completely removed from the surrounding organic matrix (Figure 3E) or partially embedded in the diffuse phase (Figure 3F-L). The low and high-resolution images revealed clusters of crystalline nano-sized particles, which make up the large wear and corrosion flakes. The insets in Figure 3E-L represent the fast-Fourier transform (FFT) patterns of the imaged nanoparticles and confirm their crystalline structure. The elemental composition of clusters and particles was determined using EDX and EELS. Elements such as Cr and O were mainly identified, along with small traces of Co and

Mo and other elements of biological origin, such as Ca and P. The Cr and O maps of a particle released from taper 1 are shown in Figure 4 and have a good match with the corresponding HAADF-STEM image (the weak maps of the other elements were not included).

The results suggest that chromium oxide with a minimum Co and Mo content is the major products released from these CoCrMo interfaces. The confirmation of the exact type of chromium oxide was obtained from the SAED investigation. The indexed SAED pattern in Figure 3A (see inset) matches the Cr_2O_3 phase, which is the most common and stable form of chromium oxide. The Cr_2O_3 structure was identified by SAED in three different clusters released from taper 1 and two clusters from stem 1.

The analytical characterisation of debris from taper 1 (one cluster) and stem 1 (three clusters) was also performed using EELS. The EELS spectra of the investigated clusters and Cr_2O_3 standard material are shown in Figure 5. The O K and Cr $L_{2,3}$ core-loss edges at 532 and 577 eV respectively, shown in Figure 5, match well for the samples and the commercial Cr_2O_3 standard material. The shift to higher energy loss peaks, observed here for Cr, has been previously reported for other transition metals and their oxides, and can be explained by the increase of the metal oxidation state. The quantitative EELS analyses, shown in Table 3, yielded to Cr and O compositions and ratios that are consistent with Cr_2O_3.The variations from the 0.66 Cr/O atomic ratio, characteristic to the pristine Cr_2O_3 species, occurred for all the samples including the standard Cr_2O_3 material, and may have been caused by the quantification errors or sample related factors, such as uneven sample thickness or the presence of contamination. A Cr/O ratio of 0.74 has been previously reported as a reliable evidence of the Cr_2O_3 phase[45]. Here, the quantitative analysis of one cluster yielded to a Cr/O ratio close to 0.66 and other clusters had ratios above 0.74. The average ratios of the four clusters, however, is 0.73 and confirms the presence of Cr_2O_3 species in debris released from taper 1 and stem 1.

STXM analysis

The STXM XANES measurements were used to identify the speciation of metal within the particles released *in vivo* from taper 2 and stem 2. The spectra shown in Figure 6, correspond to the Cr $L_{2,3}$-edges of the standard Cr_2O_3 and CrH_8O_8P materials, and debris from the retrievals. For each sample, three different clusters were investigated and the linear combination fitting yielded to a good match between the spectra of the particles and that of the commercially available Cr_2O_3 and both stem and taper showed the characteristic L edge at 579.2 eV. The edge peaks of the samples (579.2 eV), however, appeared at higher energies

compared to the edge peak of the standard Cr_2O_3 (579 eV) and at lower energies compared to the edge peak of the standard CrH_8O_8P (579.4 eV). The CrH_8O_8P standard showed particular spectral features at 582.2 eV and 589.2 eV, which are missing in the spectra of the investigated debris resulting in the better it with the Cr_2O_3 spectra. The shift of the edge peaks however, could be justified by the presence of both Cr_2O_3 and CrH_8O_8P in the partially digested flakes.

Particle size and morphology in relation to origin of debris

The size distributions of the particles released from each taper-stem couple (i.e. taper and cement-stem interface of the same implant retrieval) are shown in Figure 7A and B. The particles originating from tapers have significantly wider size distributions and larger mean and median d_{max} than the particles released from the corresponding stem interfaces ($p<0.001$ and $p<10^{-8}$ for taper-stem 1 and taper-stem 2 respectively). The comparison between the particles from taper 1 and taper 2, and stem 1 and stem 2 respectively, showed no significant differences between their size distributions ($p=0.7$ for tapers and $p=0.5$ for stems). Comparison of the size distributions of the particles from the tapers and the stems (Figure 6C) showed significant differences between the taper and stem debris ($p<10^{-10}$). The size ranges, the mean and median d_{max} and the number of particles used for the investigation of each sample, are shown in Table 4. The particles from all tapers and stems were in the nanometre size range, with none larger than 70 nm.

The morphology study shows that most of the particles released from tapers and cement-stem interfaces are mainly round or oval, with few needle shaped-particles. The results are summarised in Table 5 and show that more oval particles were released from tapers, compared to the particles released from the cement-stem interface, which were mainly round. Several dendritic, flower-like particles, like those shown in Figure 2A and D, were observed in debris from both tapers and cement-stem interfaces, but the method used here to assess the morphology (i.e. based on the particle AR), likely classified these particles as round or oval.

Particle size and composition in relation to morphology

The mean sizes of the round, oval and needle-shaped particles released from each taper and stem are shown in Table 6. The round particles are the smallest and the particle sizes increase for the oval and needle shaped debris. The statistical analysis, however, only showed significant differences between the sizes of the round and needle ($p<0.05$), and oval and needle-shaped particles ($p<0.05$) originating from stem 1, and between the round and needle-shaped particles released from taper 2 ($p<10^{-5}$). The percentage of needle-shaped particles varies from

1 to 8% for all the samples, while the round and oval debris is more abundant (see Table 5) and the statistical differences may be a consequence of the small number of particle in the needle-shaped category.

The average composition (amount of Cr, Co and Mo) of the round and oval particles released from both tapers and both stems are shown in Table 7. The results were obtained from the STEM/EDX quantitative analysis of 5 to 11 particles from each wear site and morphology type, and did not include needle-shaped particles, which are more difficult to find to gain enough data for the statistical analysis. The comparison between the composition of the round and oval particles from the same source (i.e. round vs oval particles from tapers and round vs oval particles from stems) showed no significant differences ($p>0.1$ for both tapers and stems). Similarly, the comparison between the composition of the particles with the same morphology but with different origin (i.e. round particles from tapers vs round particles from stems and oval particles from tapers vs oval particles from stems) showed no significant differences between the mean Cr, Co and Mo amounts ($p>0.5$ for round particles and $p>0.1$ for oval particles).

Discussion

The low resolution characterisation techniques used in previous studies to characterise metal debris, provided general information about the morphology and composition of the micron-sized wear and corrosion flakes, observed around the retrieved implants[15, 32, 37]. The ICP-MS technique used in this study and in one of the previous works, gave information about the metals (type and amount) in these organo-metallic composites, but failed as a method to compare the characteristics of debris released from different wear sites. To understand the factors that are involved in the particle toxicity, the metal debris has to be released from the surrounding biological matrix, by methods that preserve the particles native properties. The detailed investigation of the digested flakes and the comparison between the isolated nanoparticles in the present study, revealed some differences between the physicochemical characteristics of debris released from CoCrMo tapers and cement-stem interface. Although both interfaces produce particles in the nanometre size range, most of them were smaller than 20 nm, metal particles originating from the stems were significantly smaller than those released from the corresponding tapers. The proportion of round, oval and needle-shaped particles also varied with the origin, but the size of the particle in relation to morphology did not show significant differences for the major morphology groups (round and oval). These differences may be caused by the particular conditions at the taper and cement-stem interfaces. The cemented stems release material by micromotion between the hard ZrO_2 clusters, localised at

the surface of the cement mantle, and the proximal region of the CoCrMo stem. This results in the release of flakes from the surface of the stem, which are then entrapped at the cement-stem interface and are subject to repeated loading conditions. The cyclic steps proposed by Bryant et al. to describe the fretting corrosion at the cement-stem interface could result in a resizing of the oxide flakes, and the generation of nanoparticles. The two taper interfaces in this study were formed of femoral head components from two different manufacturers fixed to stems from a third manufacturer. This mixing has been shown to influence the probability of revision[11] and the combination may have influenced the damage mechanism. However previous retrieval analysis[46] from the same joint pairings studied in this work indicated that the levels of loss were not increased above those of other large diameter metal on metal joints. Most of the taper-trunnion debris investigated in the present study was found at the base of trunnion, outside the contacting area. This suggests that the ions and particles released at the crevice might be flushed out from the crevice space, forming organo-metallic deposits around the male taper. While there was no particle size difference between the toggling (case 2) and non-toggling (case 1) tapers, there was a difference in the composition of the undigested flakes. The corrosion dominated mechanism (case 1) was characterised by increased levels of Co and Mo compared to Cr, while debris from a toggling head (case 2) (dominated by mechanical wear) showed more Cr than Co or Mo. The study by Hothi et al.[47] investigated the link between blood metal ion levels and taper damage, and indicated that high whole blood Co/Cr ratios are indicative of taper corrosion. This finding is supported by Case 1 where a corrosion dominated mechanism of materials loss resulted in a whole blood Co/Cr ratio of 5.1. However, Case 2 had a higher level of taper loss (3.479mm^3 vs. 3.291mm^3) but the whole blood Co/Cr ratio was 1.46. This indicates that the damage mechanism, toggling vs. non-toggling, may influence the state (ionic or particulate) in which the material is released and the resultant measured ion levels.

At equal volumes of debris, the small particles show an increased specific area compared to the large particles, which makes them more susceptible to dissolution. CoCrMo debris originating from hip replacements can release Cr and Co ions by corrosion. Co^{2+} is listed among the carcinogenic compounds, and is believed to be the culprit for ALTRs and systemic manifestations[48, 49]. Cr^{3+} is the most thermodynamically stable form of Cr, but other species such as Cr^{2+} or Cr^{6+} can result from the *in vivo* redox processes. Among these species, Cr^{6+} has a well-documented cytotoxicity and genotoxicity, but its presence in the body, following hip

replacements, has never been reported. Cr^{6+} is an unstable form of Cr, and tends to be rapidly reduced to the more stable Cr^{3+}.

Here, the composition and phase analyses using EELS, SAED and XANES identified only Cr^{3+} from both CoCrMo tapers and cement-stem interfaces. The composition and chemistry (phase) did not differ with the origin, nor with the particle morphology. For the EELS and XANES analysis, the particles were still partially embedded in the surrounding matrix, which may have interfered with the investigations. The EELS provided Cr/O ratios below or above the ratio of the pure Cr_2O_3 phase. The results however were consistent with previous studies which reported a similar ratio for the Cr_2O_3 phase[45]. A more efficient dissolution of the surrounding matrix and thus cleaner particles for the EELS analysis could be achieved by using other digestion protocols such as an alkaline treatment[39, 44]. XANES analysis compared the spectra of the samples with those of pristine Cr_2O_3 and CrH_8O_8P, and the linear fitting showed a better match with the oxide phase however, the shift of the edge peaks could be justified by the presence of both Cr oxide and phosphate species in the partially digested flakes.

The spatial resolution of the I08 beamline (Diamond Source Ltd. Harwell, Science and Innovation campus, UK) is ~20 nm, but this wasn't achieved in this study. The clusters analysed had a dmax of 1-5 μm and were therefore larger than the individual nanoparticles investigated with STEM, SAED and EDX, which were completely released from the organic matrix. The STEM and EDX analysis of the cleaned nanoparticles originating from the taper and stem 2 did not show any P. It is possible therefore, that the larger clusters characterised with EELS, STXM and XANES contained Cr_2O_3 nanoparticles embedded in a matrix of organic material and Chromium Phosphate. The cleaning procedure used here might be the reason why there was no evidence of Chromium Phosphate in the high resolution imaging studies, as the Chromium Phosphate was within the matrix surrounding the Cr_2O_3 particles in a non-particulate form which was then removed. The existence of Chromium Phosphate in an amorphous state in debris from tapers is supported by the SAED work of Wang [50], which demonstrated no detectable crystalline structure within debris identified as containing Cr, P and O.

The presence of Chromium Phosphate, Cr_2O_3 and CoCr particles in tissue samples from around failing hip prostheses with evidence of damage at the tapers[32, 41-43, 50] and cement-stem interfaces[14] has been previously reported. The conditions within the crevice[51] and in the lysosomal compartment inside macrophages can favour particle dissolution and formation of

phosphate precipitates, which have been previously found in periprosthetic tissue around hip implants[33, 43]. The debris investigated in these previous studies, was not processed to release and clean the metal nanoparticles and the imaging and characterisation was undertaken at the lower resolution and thus did not reveal the characteristics of the Cr_2O_3 nanoparticles, identified in this study.

The fragments used for the ICP-MS analysis may also not reflect the composition of the flake digested and characterised with the electron microscopy techniques. ICP-MS is a destructive analytical technique and thus the flake used to determine the composition cannot be retrieved and further used for the detailed structural characterisation.

Conclusions

The results of the present study suggest that the processes occurring at the interfaces within hip replacements can influence the resultant products which are released. More mechanically driven processes result in a greater ratio of Cr to Co or Mo within the corrosion flakes. Both CoCrMo tapers and cement-stem interfaces generate Cr_2O_3 nanoparticles, with the cement-stem interface generating smaller particles compared to those from tapers.

Acknowledgments

The authors would like to acknowledge the "South of England Analytical Electron Microscope" supported by EPSRC (EP/K040375/1), and Arthroplasty for Arthritis Charity UK for research support. We also gratefully acknowledge the support of the U.S. Department of Energy through the LANL/LDRD Program and the G.T. Seaborg Institute for this work. Los Alamos National Laboratory is operated by Triad National Security, LLC, for the National Nuclear Security Administration of the U.S. Department of Energy (Contract No. 89233218CNA000001). The data used in this study is available at: DOI: https://doi.org/10.5258/SOTON/D1410

References

1. Langton, D., et al., *Accelerating failure rate of the ASR total hip replacement.* The Journal of bone and joint surgery. British volume, 2011. **93**(8): p. 1011-1016.

2. Hsu, A.R., C.E. Gross, and B.R. Levine, *Pseudotumor from modular neck corrosion after ceramic-on-polyethylene total hip arthroplasty.* American journal of orthopedics, 2012. **41**(9): p. 422.
3. Cooper, H.J., et al., *Corrosion at the head-neck taper as a cause for adverse local tissue reactions after total hip arthroplasty.* The Journal of bone and joint surgery. American volume, 2012. **94**(18): p. 1655.
4. Cooper, H.J., et al., *Adverse local tissue reaction arising from corrosion at the femoral neck-body junction in a dual-taper stem with a cobalt-chromium modular neck.* The Journal of bone and joint surgery. American volume, 2013. **95**(10): p. 865.
5. Lindgren, J., B. Brismar, and A. Wikstrom, *Adverse reaction to metal release from a modular metal-on-polyethylene hip prosthesis.* The Journal of bone and joint surgery. British volume, 2011. **93**(10): p. 1427-1430.
6. Cook, R.B., et al., *Pseudotumour formation due to tribocorrosion at the taper interface of large diameter metal on polymer modular total hip replacements.* The Journal of arthroplasty, 2013. **28**(8): p. 1430-1436.
7. Whitehouse, M., et al., *Adverse local tissue reactions in metal-on-polyethylene total hip arthroplasty due to trunnion corrosion: the risk of misdiagnosis.* The bone & joint journal, 2015. **97**(8): p. 1024-1030.
8. Chana, R., et al., *Mixing and matching causing taper wear: corrosion associated with pseudotumour formation.* The Journal of bone and joint surgery. British volume, 2012. **94**(2): p. 281-286.
9. Fricka, K.B., et al., *Metal-on-metal local tissue reaction is associated with corrosion of the head taper junction.* The Journal of arthroplasty, 2012. **27**(8): p. 26-31. e1.
10. Matthies, A.K., et al., *Material loss at the taper junction of retrieved large head metal-on-metal total hip replacements.* Journal of Orthopaedic Research, 2013. **31**(11): p. 1677-1685.
11. Tucker, K., et al., *Mixing of components from different manufacturers in total hip arthroplasty: prevalence and comparative outcomes.* Acta orthopaedica, 2015. **86**(6): p. 671-677.
12. Langton, D., et al. *Metal debris release from taper junctions appears to have a greater clinical impact than debris released from metal on metal bearing surfaces*. in *Orthopaedic Proceedings*. 2013. The British Editorial Society of Bone & Joint Surgery.
13. Sidaginamale, R., et al., *The clinical implications of metal debris release from the taper junctions and bearing surfaces of metal-on-metal hip arthroplasty: joint fluid and blood metal ion concentrations.* The bone & joint journal, 2016. **98**(7): p. 925-933.
14. Campbell, P., et al., *Autopsy analysis thirty years after metal-on-metal total hip replacement: a case report.* JBJS, 2003. **85**(11): p. 2218-2222.
15. Hothi, H.S., et al., *Clinical significance of corrosion of cemented femoral stems in metal-on-metal hips: a retrieval study.* International orthopaedics, 2016. **40**(11): p. 2247-2254.
16. Bryant, M., et al., *Characterisation of the surface topography, tomography and chemistry of fretting corrosion product found on retrieved polished femoral stems.* Journal of the mechanical behavior of biomedical materials, 2014. **32**: p. 321-334.
17. Shearwood-Porter, N., et al., *Damage mechanisms at the cement–implant interface of polished cemented femoral stems.* Journal of Biomedical Materials Research Part B: Applied Biomaterials, 2017. **105**(7): p. 2027-2033.
18. Bolland, B., et al., *High failure rates with a large-diameter hybrid metal-on-metal total hip replacement: clinical, radiological and retrieval analysis.* The Journal of bone and joint surgery. British volume, 2011. **93**(5): p. 608-615.
19. Donell, S., et al., *Early failure of the Ultima metal-on-metal total hip replacement in the presence of normal plain radiographs.* The Journal of bone and joint surgery. British volume, 2010. **92**(11): p. 1501-1508.

20. Cook, R.B., et al., *Volumetric assessment of material loss from retrieved cemented metal hip replacement stems.* Tribology International, 2015. **89**: p. 105-108.
21. Goldberg, J.R. and J.L. Gilbert, *In vitro corrosion testing of modular hip tapers.* Journal of Biomedical Materials Research Part B: Applied Biomaterials: An Official Journal of The Society for Biomaterials, The Japanese Society for Biomaterials, and The Australian Society for Biomaterials and the Korean Society for Biomaterials, 2003. **64**(2): p. 78-93.
22. Bryant, M., et al., *Failure analysis of cemented metal-on-metal total hip replacements from a single centre cohort.* Wear, 2013. **301**(1-2): p. 226-233.
23. Bryant, M., et al., *Fretting corrosion characteristics of polished collarless tapered stems in a simulated biological environment.* Tribology International, 2013. **65**: p. 105-112.
24. Brown, C., et al., *Characterisation of wear particles produced by metal on metal and ceramic on metal hip prostheses under standard and microseparation simulation.* Journal of Materials Science: Materials in Medicine, 2007. **18**(5): p. 819-827.
25. Pourzal, R., et al., *Characterization of wear particles generated from CoCrMo alloy under sliding wear conditions.* Wear, 2011. **271**(9-10): p. 1658-1666.
26. Catelas, I., et al., *Comparison of in vitro with in vivo characteristics of wear particles from metal–metal hip implants.* Journal of Biomedical Materials Research Part B: Applied Biomaterials: An Official Journal of The Society for Biomaterials, The Japanese Society for Biomaterials, and The Australian Society for Biomaterials and the Korean Society for Biomaterials, 2004. **70**(2): p. 167-178.
27. Goode, A.E., et al., *Chemical speciation of nanoparticles surrounding metal-on-metal hips.* Chemical Communications, 2012. **48**(67): p. 8335-8337.
28. Hart, A.J., et al., *The chemical form of metallic debris in tissues surrounding metal-on-metal hips with unexplained failure.* Acta biomaterialia, 2010. **6**(11): p. 4439-4446.
29. Doorn, P.F., et al., *Metal wear particle characterization from metal on metal total hip replacements: transmission electron microscopy study of periprosthetic tissues and isolated particles.* Journal of Biomedical Materials Research: An Official Journal of The Society for Biomaterials, The Japanese Society for Biomaterials, and the Australian Society for Biomaterials, 1998. **42**(1): p. 103-111.
30. Billi, F., et al., *The John Charnley award: an accurate and extremely sensitive method to separate, display, and characterize wear debris part 2: metal and ceramic particles.* Clinical Orthopaedics and Related Research®, 2012. **470**(2): p. 339-350.
31. Billi, F., et al., *Metal wear particles: What we know, what we do not know, and why.* International Journal of Spine Surgery, 2009. **3**(4): p. 133-142.
32. Urban, R.M., et al., *Migration of corrosion products from modular hip prostheses. Particle microanalysis and histopathological findings.* The Journal of bone and joint surgery. American volume, 1994. **76**(9): p. 1345-1359.
33. Urban, R.M., et al., *Dissemination of wear particles to the liver, spleen, and abdominal lymph nodes of patients with hip or knee replacement.* JBJS, 2000. **82**(4): p. 457.
34. Urban, R.M., et al., *Accumulation in liver and spleen of metal particles generated at nonbearing surfaces in hip arthroplasty.* The Journal of arthroplasty, 2004. **19**(8): p. 94-101.
35. Case, C., et al., *Widespread dissemination of metal debris from implants.* The Journal of bone and joint surgery. British volume, 1994. **76**(5): p. 701-712.
36. Langkamer, V., et al., *Systemic distribution of wear debris after hip replacement. A cause for concern?* The Journal of bone and joint surgery. British volume, 1992. **74**(6): p. 831-839.
37. Scharf, B., et al., *Molecular analysis of chromium and cobalt-related toxicity.* Scientific reports, 2014. **4**: p. 5729.
38. Kavanaugh, A., P. Benya, and F. Billi, *A method to isolate and characterize wear debris from synovial fluid and tissues*, in *Metal-On-Metal Total Hip Replacement Devices*. 2013, ASTM International.

39. Catelas, I., et al., *Effects of digestion protocols on the isolation and characterization of metal–metal wear particles. I. Analysis of particle size and shape.* Journal of Biomedical Materials Research: An Official Journal of The Society for Biomaterials, The Japanese Society for Biomaterials, and The Australian Society for Biomaterials and the Korean Society for Biomaterials, 2001. **55**(3): p. 320-329.
40. Catelas, I., et al., *Effects of digestion protocols on the isolation and characterization of metal–metal wear particles. II. Analysis of ion release and particle composition.* Journal of Biomedical Materials Research: An Official Journal of The Society for Biomaterials, The Japanese Society for Biomaterials, and The Australian Society for Biomaterials and the Korean Society for Biomaterials, 2001. **55**(3): p. 330-337.
41. Xia, Z., et al., *Nano-analyses of wear particles from metal-on-metal and non-metal-on-metal dual modular neck hip arthroplasty.* Nanomedicine: Nanotechnology, Biology and Medicine, 2017. **13**(3): p. 1205-1217.
42. Munir, S., et al., *The histological and elemental characterisation of corrosion particles from taper junctions.* Bone & joint research, 2016. **5**(9): p. 370-378.
43. Di Laura, A., et al., *The chemical form of metal species released from corroded taper junctions of hip implants: synchrotron analysis of patient tissue.* Scientific reports, 2017. **7**(1): p. 1-13.
44. Crainic, A.M., et al., *I nvestigation of nano-sized debris released from CoCrMo secondary interfaces in total hip replacements: D igestion of the flakes.* Journal of Biomedical Materials Research Part B: Applied Biomaterials, 2019. **107**(2): p. 424-434.
45. De Castro, V., et al., *Oxide dispersion strengthened Fe–12Cr steel in three dimensions: An electron tomography study.* Journal of nuclear materials, 2014. **444**(1-3): p. 416-420.
46. Cook, R.B., J.M. Latham, and R.J.K. Wood, *The Performance of Mixed Manufacturer Metal On Metal Total Hip Replacements.* Reconstructive Review, 2017. **7**(2).
47. Hothi, H.S., et al., *The Relationship Between Cobalt/Chromium Ratios and the High Prevalence of Head-Stem Junction Corrosion in Metal-on-Metal Total Hip Arthroplasty.* The Journal of Arthroplasty, 2016. **31**(5): p. 1123-1127.
48. Bradberry, S., J. Wilkinson, and R. Ferner, *Systemic toxicity related to metal hip prostheses.* Clinical toxicology, 2014. **52**(8): p. 837-847.
49. Cheung, A., et al., *Systemic cobalt toxicity from total hip arthroplasties: review of a rare condition Part 1-history, mechanism, measurements, and pathophysiology.* The bone & joint journal, 2016. **98**(1): p. 6-13.
50. Wang, Q., *Corrosion associated failure mechanisms of CoCrMo alloys in total hip replacements*. 2019.
51. Gibon, E., et al., *The biological response to orthopaedic implants for joint replacement: Part I: Metals.* Journal of Biomedical Materials Research Part B: Applied Biomaterials, 2017. **105**(7): p. 2162-2173.

Figure Legends

Figure 1: Retrieved femoral components with wear and corrosion products (arrows) Case 1: A and B, Case 2: C and D.

Figure 2: RedLux height map images of the taper surface showing the material loss a different mechanisms of loss from the taper.

Figure 3: The HAADF-STEM micrographs of partially digested flakes and particles released from (A, E, I) taper 1; (B, F, G) stem 1; (C, G, K) taper 2; (D, H, L) stem 2. The inset in Fig. 2A represents the SAED pattern of a cluster of Cr_2O_3 nanoparticles, while the insets in Fig. 2E-L are FFT patterns and show the particles are crystalline.

Figure 4: The HAADF-STEM micrograph and the Cr and O map of representative particles released from CoCrMo tapers and cement-stem interface.

Figure 5: The EELS spectra of a standard Cr_2O_3 sample and debris from taper 1 and stem 1, showing the O K edge and Cr $L_{2,3}$ peaks at 532 and 577 eV respectively.

Figure 6: The representative Cr $L_{2,3}$ XANES spectra of debris from taper 2, stem 2 and standard Cr_2O_3 and $CrPO_4$ material.

Figure 7: The PSDs of debris released from CoCrMo tapers (blue) and cement stem interface (red). (A) shows the PSDs of particles originating from stem 1 and taper 1 and the corresponding mean sizes; (B) shows the PSDs and mean sized of debris from stem 2 and taper 2; (C) shows the PSDs and mean sizes of particles from all stems and all tapers. $p<0.001$*; $p<10^{-8}$**.


A


B

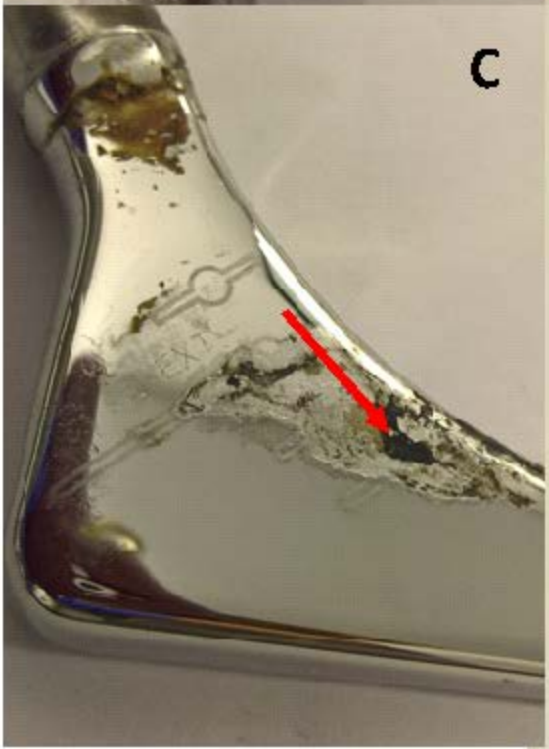
C


D

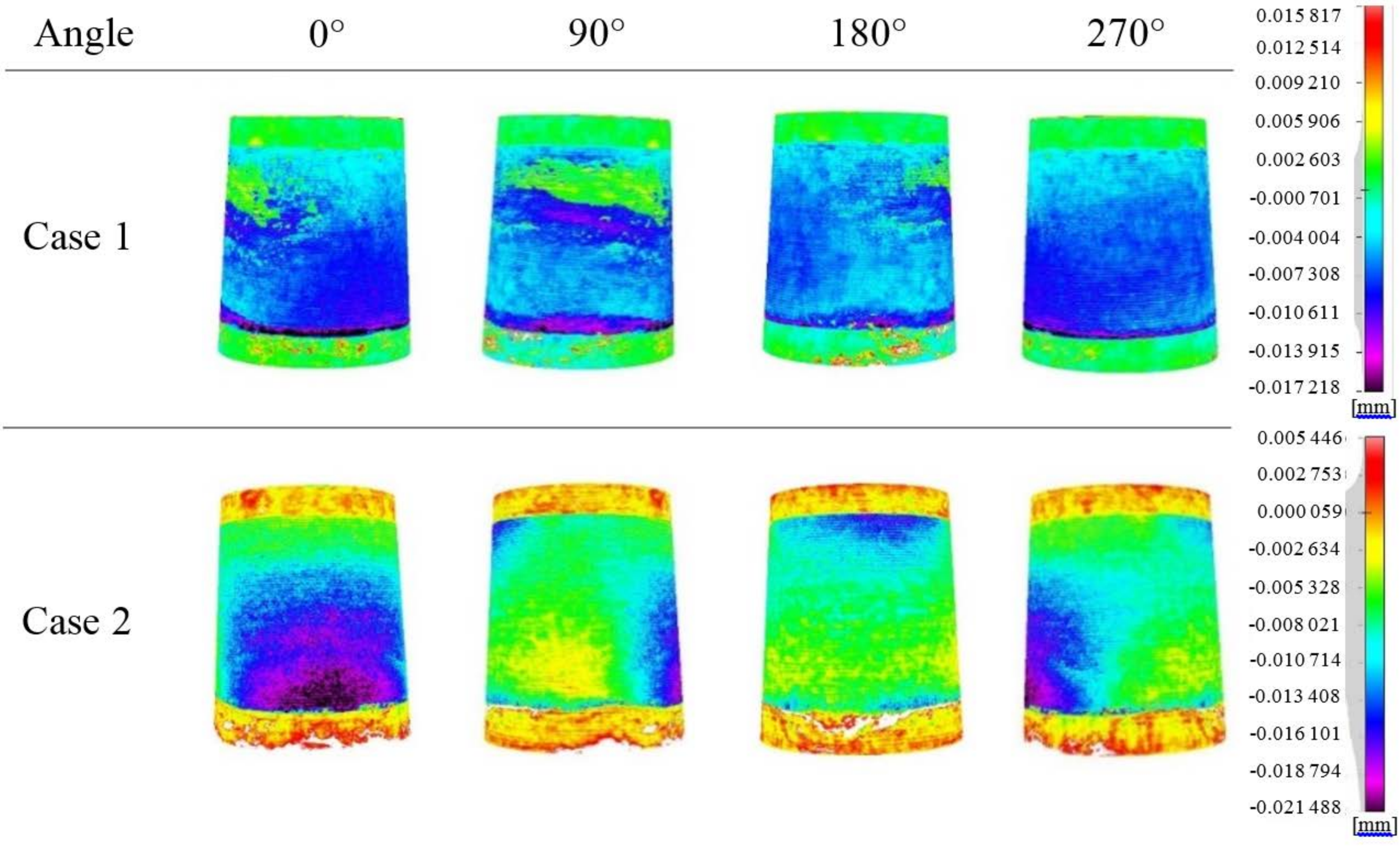
Angle
0°
90°
180°
270°
Case 1
Case 2
0.015 817
0.012 514
0.009 210
0.005 906
0.002 603
-0.000 701
-0.004 004
-0.007 308
-0.010 611
-0.013 915
-0.017 218
[mm]
0.005 446
0.002 753
0.000 059
-0.002 634
-0.005 328
-0.008 021
-0.010 714
-0.013 408
-0.016 101
-0.018 794
-0.021 488
[mm]

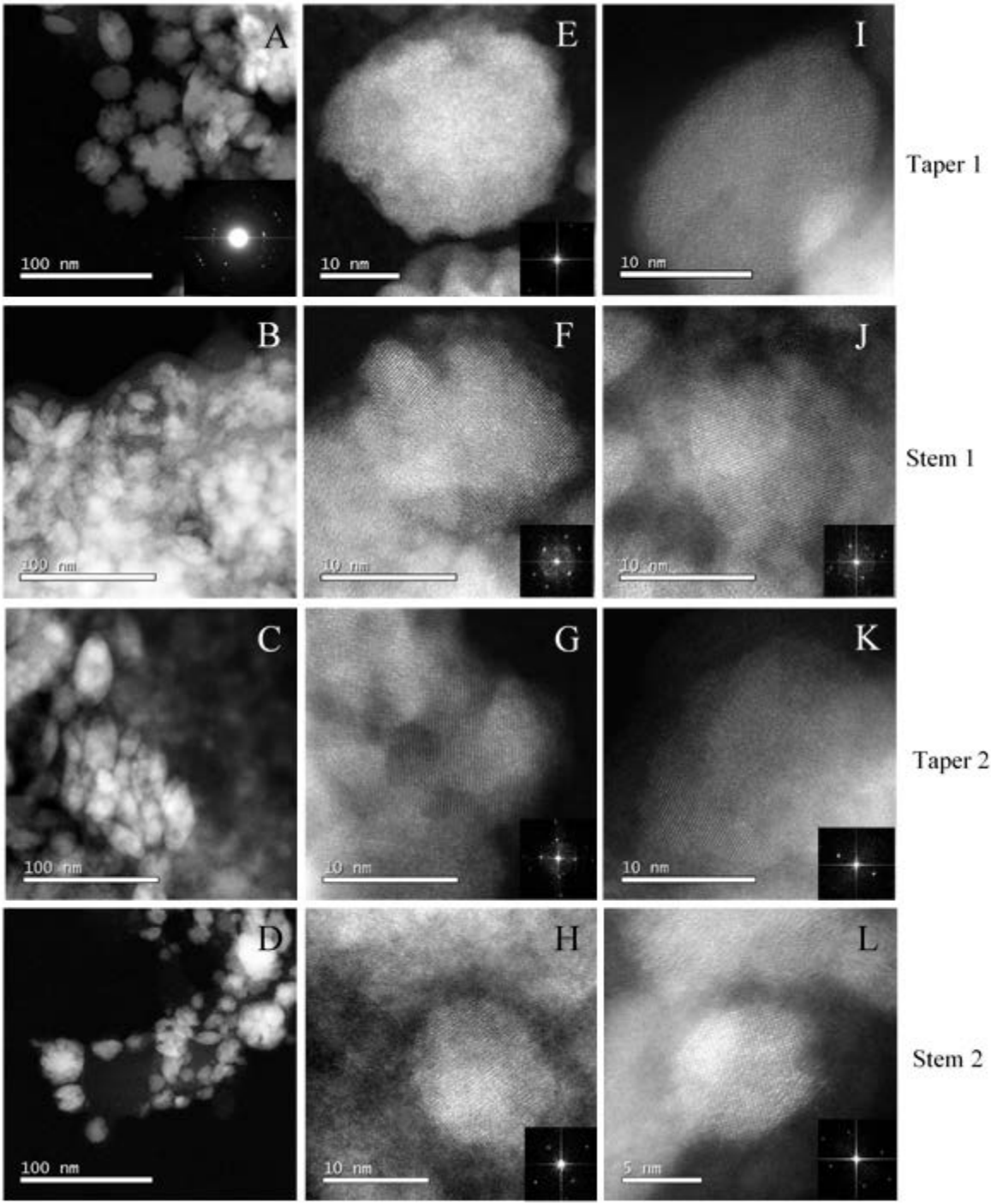
A
E
I
Taper 1
100 nm
10 nm
10 nm
B
F
J
Stem 1
100 nm
10 nm
10 nm
C
G
K
Taper 2
100 nm
10 nm
10 nm
D
H
L
Stem 2
100 nm
10 nm
5 nm

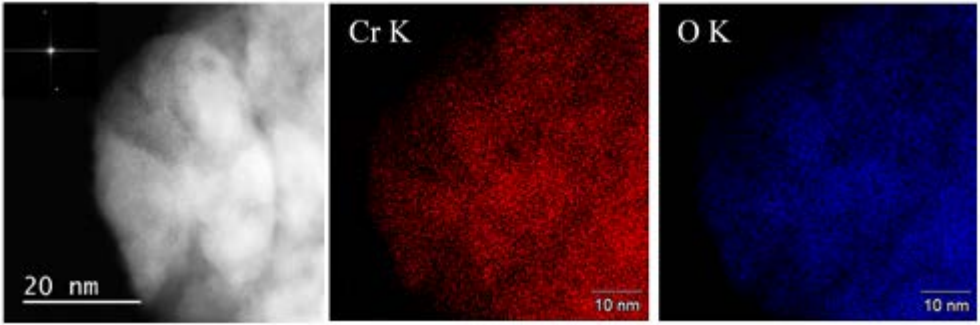
20 nm
Cr K
10 nm
O K
10 nm

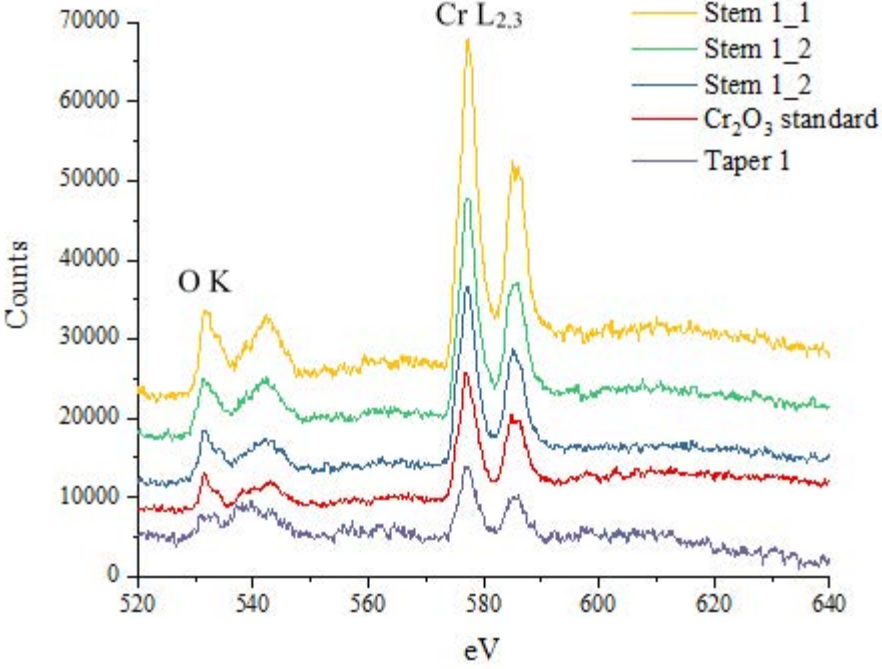
Cr L2,3
O K
Stem 1_1
Stem 1_2
Stem 1_2
Cr2O3 standard
Taper 1
Counts
eV
70000
60000
50000
40000
30000
20000
10000
0
520
540
560
580
600
620
640

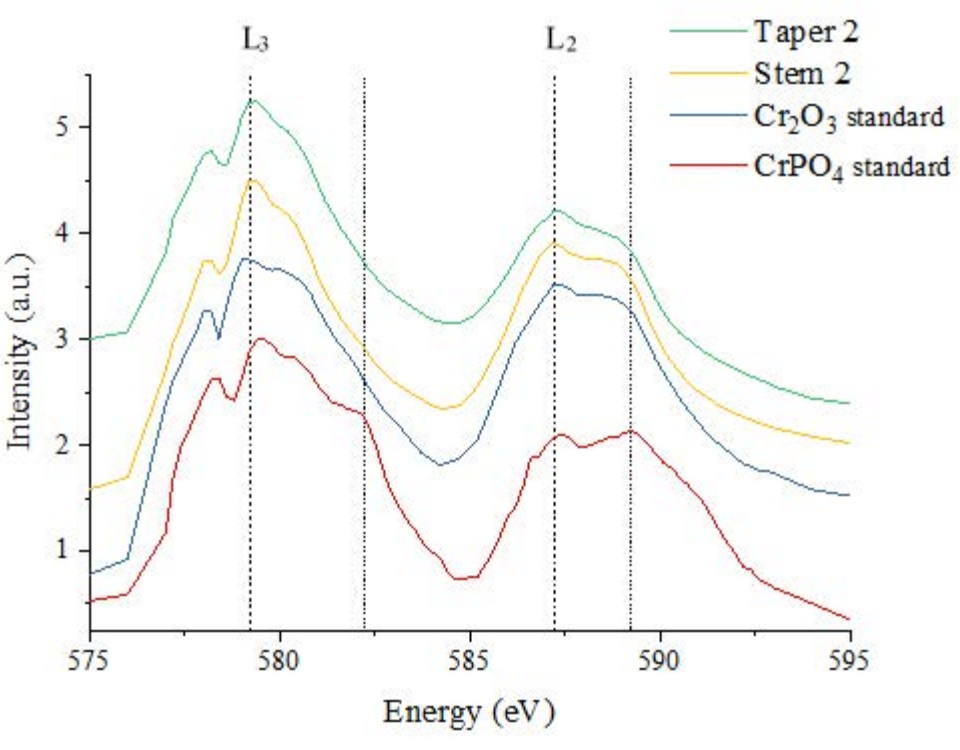
L3
L2
Taper 2
Stem 2
Cr2O3 standard
CrPO4 standard
Intensity (a.u.)
1
2
3
4
5
575
580
585
590
595
Energy (eV)

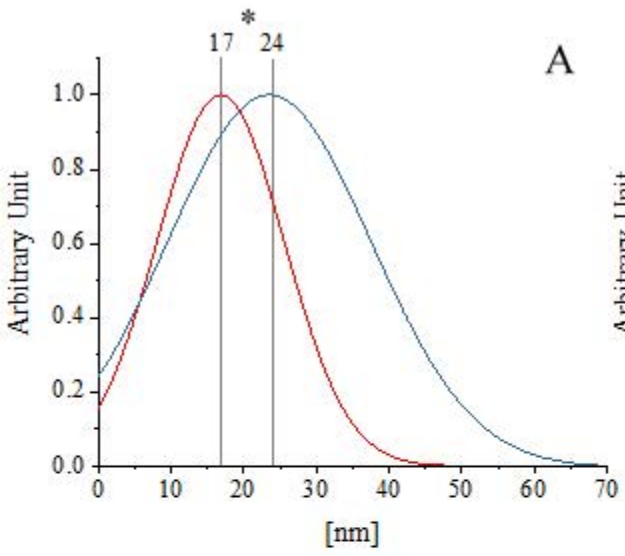
*
17
24
A
Arbitrary Unit
1.0
0.8
0.6
0.4
0.2
0.0
0
10
20
30
40
50
60
70
[nm]

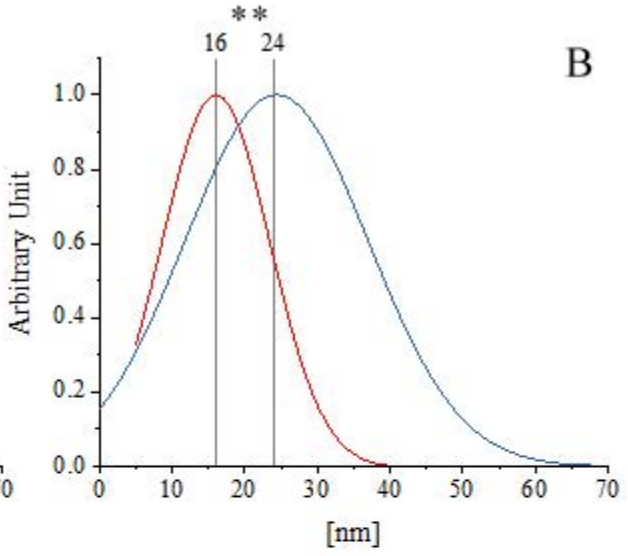
**
16
24
B
Arbitrary Unit
1.0
0.8
0.6
0.4
0.2
0.0
0
10
20
30
40
50
60
70
[nm]

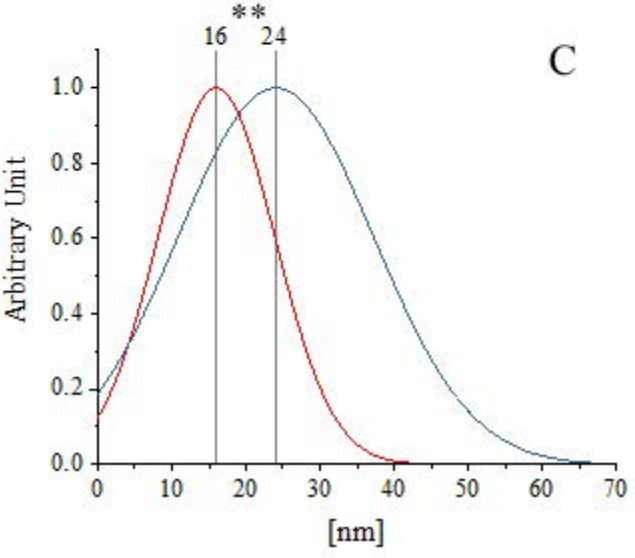
**
16
24
C
Arbitrary Unit
1.0
0.8
0.6
0.4
0.2
0.0
0
10
20
30
40
50
60
70
[nm]

Table 1: Information about the patients and implants used in the study.

	Case 1	**Case 2**
Head make	Adept (cast, heat treated)	BHR (cast)
Head size and offset (mm)	46+0	50+4
Taper make	CPT (wrought)	CPT (wrought)
Taper size (mm)	12/14	12/14
Age at Primary (years)	62	58
Time In-Vivo (months)	113	101
Blood Co Ions (nmol/l)	6520	102
Blood Cr Ions (nmol/l)	1450	69.9
Bearing Combined Wear Rate (mm^3/yr)	0.42	0.683

Table 2: The amount of Cr, Co and Mo, and the total percentage of metal within the undigested flakes.

Sample	**Cr%**	**Co%**	**Mo%**	**Total Metal %**
Taper 1	5.9	7.8	6.1	19.8
Stem 1	14.5	2.3	2.0	18.8
Taper 2	29.2	5.6	3.1	37.9
Stem 2	10.1	2.3	1.5	13.9

Table 3: Cr/O ratio and composition of Cr_2O_3 standard material and debris from taper 1 and stem 1, obtained from the quantitative EELS analysis.

Sample	**O (at.%)**	**Cr (at.%)**	**Cr/O**
Cr_2O_3	50.3±1.1	49.7±1.1	0.99
Stem 1_1	56.5±1	43.5±1	0.77
Stem 1_2	61.2±2	38.8±2	0.63
Stem 1_3	54.9±0.4	45.1±0.4	0.82
Taper 1	58.6±1.5	41.2±1.5	0.71

Table 4: The number of particles used for the size distributions, the size ranges and the mean and median d_{max} for each taper and stem, and all tapers and all stems.

Sample	**No of particles**	**Size range**	**Mean d_{max}**	**Median d_{max}**
Taper 1	75	4-64 nm	24 nm	20 nm
Stem 1	85	4-49 nm	17 nm	16 nm
Taper 2	107	6-67 nm	24 nm	22 nm
Stem 2	115	6-37 nm	16 nm	14 nm
All tapers	182	4-67 nm	24 nm	21 nm
All stems	200	4-49 nm	16 nm	15 nm

Table 5: The results of the morphology study, indicating the % of round, oval and needle shaped particles for each taper and stem sample.

Sample	**Round %**	**Oval %**	**Needle shaped %**
Taper 1	48	49	3
Stem 1	54	41	5
Taper 2	39	53	8
Stem 2	72	27	1

Table 6: The mean sizes of the round, oval and needle-shaped particles released from tapers and stems.

*significant difference between oval and needle ($p<0.05$) and round and needle ($p<0.05$)

**significant difference between round and needle ($p<10^{-5}$)

Sample	**Mean d_{max}**		
	Round	*Oval*	*Needle-shaped*
Taper 1	21 nm	25 nm	37 nm
Stem 1*	15 nm	19 nm	23 nm
Taper 2**	21 nm	26 nm	32 nm
Stem 2	15 nm	18 nm	25 nm

Table 7: The average composition of round and oval particles released from tapers and stems, resulted from STEM/EDX quantitative analysis.

Sample	**Morphology**	**Composition**		
		Cr%	Co%	Mo%
Tapers	Round	82	17	1
	Oval	85	13	2
Stems	Round	84	15	1
	Oval	81	18	1